Enhanced electrocatalytic activity of copper phthalocyanine/multiwalled carbon nanotube composite electrode via Pt nanoparticle modification for oxygen reduction

Çağrı Ceylan KOÇAK[1], Zekerya DURSUN[2],*

[1]Bergama Vocational School, Dokuz Eylül University, İzmir, Turkey
[2]Department of Chemistry, Faculty of Science, Ege University, Bornova, İzmir, Turkey

Abstract: Enhanced electrocatalytic reduction of oxygen is achieved using Pt nanoparticle-modified copper phthalocyanine-multiwalled carbon nanotube (PtNPs/CuPc-CNT) composite film on a glassy carbon electrode (PtNPs/CuPc-CNT/GCE). The PtNPs/CuPc-CNT/GCE surface is characterized by scanning electron microscopy, transmission electron microscopy, electrochemical impedance spectroscopy, X-ray photoelectron spectroscopy, and X-ray diffraction. The electrocatalytic activity of composite electrodes in the oxygen reduction reaction is investigated by cyclic voltammetry and rotating-disk electrode measurements. PtNPs/CuPc-CNT/GCE show higher catalytic activity than CNT/GCE, CuPc/GCE, and CuPc-CNT/GCE in oxygen reduction with four electron transfers.

Key words: Oxygen reduction, platinum nanoparticles, carbon nanotube, phthalocyanine

1. Introduction

Fuel cells are clean and efficient power sources used to generate electricity from hydrogen and oxygen, and platinum (Pt) and Pt-based materials have been commonly utilized as important air-cathode catalysts in the oxygen reduction reaction (ORR). However, the use of a bulk electrode in such a system has major disadvantages as Pt is expensive and rare and can cause catalyst poisoning, which diminishes the performance of fuel cells.[1] Therefore, researchers have focused on developing alternative catalyst materials in order to address the high cost and other disadvantages. Recently, Pt metal-free materials have been studied for the reduction of oxygen, but only a few materials (copper, manganese, etc.) showed electrocatalytic activity towards this reaction with an unstable surface.[2,3] The second option to minimize the problem of high cost is to use a small amount of Pt as metal nanoparticles form on the electrode surface. Therefore, it is necessary to develop Pt deposited on substrates to increase the ORR activity and the stable electrode surface and to reduce the associated overpotential.[4,5] For this purpose, phthalocyanines (Pcs) and carbon nanotubes were widely used substrates to prepare active surfaces with metal nanoparticles towards oxygen reduction.

Pcs, synthetic analogs of porphyrins, are aromatic macrocycles that have four isoindole groups connected by nitrogen. Pcs and their metalloderivatives (MPcs) possess electrochemical and photophysical properties that make them very interesting functional molecules. Moreover, Pcs have attracted considerable attention in different areas, such as in the preparation of dyestuffs for textiles and inks, and as main parts in the

---

*Correspondence: zekerya.dursun@ege.edu.tr

construction of molecular materials for sensing analytes, liquid crystals, semiconductive materials, photovoltaic cells, and optoelectronics.[6,7] The structure of Pcs enables the preparation of a diverse variety of related structures with substantially improved physical, electronic, and optical properties. The physical responses of Pcs can be increased by incorporating various kinds of metal atoms into the Pc ring. They have a π-electron conjugation system in the metal Pc molecular structure and thus exhibit high oxidation and reduction properties.[8−12] Copper central metal was studied as an electrode component due to its catalytic activity towards many analytes.[13−15] Cu(II)-Pcs are especially common redox catalysts that have been used as candidates for exploring Pt-free ORR catalysts in fuel-cell reactions.[16] However, the major drawbacks of Pc complexes are their low stability and poor electron conductivity.[12,16] Therefore, to improve their electrocatalytic activity and stability, conductive support materials are required in the preparation of catalytic surfaces with Pc complexes. For this purpose, carbon nanotubes are great candidates as supporting material for Pcs.

Carbon nanotubes (CNTs) have also attracted extensive attention in many areas of engineering and science due to their unique chemical, mechanical, and physical properties. For example, their electric conductivity is comparable to that of copper, but their density is only about one-sixth, and their tensile strength is 100 times higher than that of stainless steel. In addition, their chemical stability and thermal conductivity are comparable to that of various diamonds.[17−19] Furthermore, CNTs have defects in the graphite structure at their end and side walls, which enables the noncovalent or covalent functionalization of CNTs to catalyze electron transfer kinetics.[20,21] For instance, MPc complexes can be covalently attached to CNTs and complexes (nonsubstituted) are adsorbed noncovalently onto the surface of CNTs by $\pi−\pi$ interactions. It has already been determined that Pc–CNT composites share the excellent catalytic activity properties of Pcs and the perfect electronic properties of carbon nanotubes.[22−25]

Studies of metal nanoparticles and nanostructures have suggested that they enhance mass transport, facilitate the electron transfer rate, control their environment, and increase the effective surface area.[26−30] In this respect, metal nanoparticles have been used in electrocatalytic reactions to facilitate electron transfer.[31] Metal nanoparticles and Pc/carbon nanotubes at the electrode surface significantly improve electrode activity.[32−34]

The cathodic ORR is the greatest performance restrictor of fuel-cell applications. Improving catalysts would thus significantly improve effect on the efficiency of the fuel cell,[35−37] and in this respect the preparation of cathode catalysts has been the focus of substantial research over the past few decades. Electrochemical oxygen reduction involves the use of two main steps: first, a two-step, two-electron pathway is used to produce hydrogen peroxide, and second, a direct four-electron pathway is used to produce water.

In an alkaline solution, the pathway involving two electrons is:

$$\mathbf{O_2 +\ H_2O\ +\ 2e^-\ \rightarrow\ HO_2^-\ +\ OH^-} \tag{1}$$

and the pathway involving direct four electrons is:

$$\mathbf{O_2 +\ 2H_2O\ +\ 4e^-\ \rightarrow\ 4OH^-} \tag{2}$$

To obtain maximum energy capacity, use of the direct four-electron pathway is highly desirable as it reduces molecular oxygen.[38−41]

The research group involved in writing this current paper has previously published papers on ORRs using the following: electrochemically prepared copper-gold nanoparticle-modified carbon nanotube/GCE,[42] Au(111) single-crystal electrode ad-layered with platinum,[43] and a single-crystal electrode modified with a Pd ad-layer.[44]

Of these, the ad-layer modified single-crystal electrodes have been shown to have higher catalytic activity towards oxygen reduction in alkaline media; however, the method has major disadvantages: the electrode material is expensive and preparation of single-crystal electrodes requires considerable expertise. It is thus considered that a new type of electrode material is required to reduce the cost of the electrocatalytic surface with respect to the reduction or oxidation of compounds.

Several research groups have recently explored the use of metal Pc functionalized carbon-based composites as the electrode materials of fuel cells.[45] For example, Zhang et al. prepared iron tetrasulfophthalocyanine functionalized graphene composites with enhanced activity for the ORR in a dual-chamber microbial fuel cell.[4]

There are many studies on Pc-based electrodes for the ORR in the literature,[46−51] but to our knowledge no previous report has been published about the use of the Pt nanoparticle-modified CuPc-CNT composite electrode in oxygen reduction.

The main objective of this work is to prepare a new extremely stable composite material of Pt-CuPc-CNT with a simple fabrication method for highly catalytic activity towards oxygen reduction in alkaline media. The Pt nanoparticles and CuPc act as an electrocatalyst for the reduction of oxygen, whereas the CNT increases the electroactive surface area, enhances the immobilization of Pt nanoparticles and CuPc, and promotes the electron transfer between the Pt-CuPc and electrode. The electrocatalytic activity of the composite electrode towards the ORR is evaluated by cyclic voltammetric, linear sweep voltammetric, and rotating-disk electrode (RDE) techniques. All composite electrodes are characterized by scanning electron microscopy (SEM), X-ray photoelectron spectroscopy (XPS), and electrochemical impedance spectroscopy (EIS). The electrocatalytic activity of the PtNPs/CuPc-CNT composite electrode is studied with respect to oxygen reduction using both static and rotating-disk electrodes in an alkaline solution.

2. Results and discussion

2.1. Preparation of Pt nanoparticle-modified CNT/GC, CuPc/GC, and CuPc-CNT/GC electrodes

CNT/GC, CuPc/GC, and CuPc-CNT/GC electrodes were prepared using the drop-dry technique as referred to in Section 3. The electrochemical deposition of Pt metal nanoparticles was performed using electrochemical reduction of 3 mM K_2PtCl_6 on the CNT/GCE, CuPc/GCE, and CuPc-CNT/GCE in 0.1 M HCl solution. All electrodes were dipped in 3 mM Pt^{4+}-containing 0.1 M HCl solution. Consecutive cyclic voltammograms (CVs) were performed using appropriate potential range windows that enabled the viewing of the reduction and oxidation peaks of platinum in relation to changes in the modification surface.

2.2. Electroactive surface area of electrodes

The electroactive surface area (ESA) is generally determined using a CV with a ferrocyanide-ferricyanide redox couple involving one electron transfer per molecule with a reversible redox characteristic.[45] In this study, CVs were recorded at various scan rates in a ferro-ferricyanide redox couple-containing solution; the square root of the scan rate versus the peak current was then plotted. The ESA can be calculated based on the Randles–Sevcik equation as follows:

$$\times i_p = \left(2.69 10^5\right) n^{3/2} A\, C\, D^{1/2} v^{1/2} \tag{3}$$

Here, n is the number of electrons transferred in the redox process, A is the active area of the electrode (cm^2), D is the diffusion coefficient $(cm^2\ s^{-1})$, C is the concentration of electroactive species $(mol\ cm^{-3})$, and v is

the scan rate value (V s^{-1}). The ferro-ferricyanide system involves the transfer of one electron; therefore, the n value was taken as 1, D is 6.70 $\times$ 10^{-5} cm^2 s^{-1},[52] the ferro-ferricyanide concentration (C) used was 10^{-6} mol cm^{-3}, and scan rate studies were conducted for all bare and modified electrodes (10–350 mV s^{-1}). If the slope value of the square root of the scan rate versus the peak current plot was then replaced into the equation, the only unknown component in the equation was that of A, which could then be calculated. To investigate the ESA of bare and modified electrodes, the CVs were recorded with different scan rates in 1.0 mM K$_4$Fe(CN)$_6$+ 0.1 M KCl solution. From the slope of the linear graph line, the electroactive areas of the GCE, CuPc-CNT/GCE, PtNPs/CNT/GCE, PtNPs/CuPc/GCE, and PtNPs/CuPc-CNT/GCE were calculated as 0.056, 0.280, 0.57, 0.087, and 0.84 cm^2, respectively. The results show that the entire geometric area of the bare GCE exhibited poor electrochemical activity, which is in good agreement with reported data.[53] CNTs are tubular nanostructures that cause an increase in the surface area of smooth surfaces. The same behavior is observed when macrocyclic Pcs are modified on poorly active surfaces like GCE. ESA values of PtNPs/CNT/GCE and PtNPs/CuPc/GCE were found higher than those of their Pt-free forms. This behavior can be attributed to the active platinum sides distributed all over these surfaces in nanometer size. In addition, the highest ESA value was calculated for PtNPs/CuPc-CNT/GCE, which means it is the most active surface towards the analyte. PtNPs modification on both tubular and macrocyclic surfaces together leads to an increase in the active surface area, which is in accordance with CV results. This high value can be attributed to the synergistic effect of the presence of PtNPs, CuPc, and CNT on the GCE surface. The drastic difference between ESA values of PtNPs/CuPc/GCE and PtNPs/CuPc-CNT/GCE shows the contribution of CNTs to active surface area such that the choice of CNT as a component is meaningful. In brief, the larger ESA provided higher current values than that obtained for oxygen reduction in the same order.

2.3. Characterization of electrodes

The surface morphology of all electrodes was characterized using SEM. As shown in Figure 1, the SEM image of the acid-treated CNT (Figure 1a) can be explained by the smooth and rather uniform pattern of CNTs distributed on the GCE surface. In Figure 1b, the composition of CuPc on the CNT/GCE is seen as round-shaped, bright, and dispersed homogeneously. In Figure 1c, almost uniformly distributed PtNPs (size 10–100 nm), which are seen as bright dots, indicate that electrochemical synthesis was successful. A comparison between Figure 1b and Figure 1c (before and after Pt nanoparticle deposition) reveals an obvious observable change in the distribution of particle sizes on the CuPc–CNT surface. To qualitatively confirm the composite electrode surface composition, the prepared PtNPs/CuPc–CNT/GCE was characterized using energy-dispersive x-ray spectroscopy (EDX) (Figure 1d), which proved that electrodeposition of Pt nanoparticles on the CuPc–CNT/GC surface was successful. In addition, the weight gain of CuPc–CNT due to Pt loading is about 9.7%, and N and Cu atoms have the structure of a copper Pc molecule.

Transmission electron microscopy (TEM) images of CuPc/CNT/GCE and PtNPs/CuPc-CNT/GCE catalysts are shown in Figure 2. Typical TEM images assist in understanding the morphology and differences in particle size before and after the deposition of platinum nanoparticles. Figures 2a–2f show micrographs of the CuPc-CNT/GCE precursor, where a clean surface is visible with CuPc particles evenly dispersed on the carbon nanotubes. It can be seen that most of the Pt nanoparticles are uniformly dispersed in the range of 3–6 nm on the CuPc-CNT/GCE support (Figures 2g–2l). After platinum deposition, aggregates (such as Pt-containing cluster compounds) appear on the CuPc-modified CNTs. However, in comparison with the CuPc precursor, a number of Pt-containing cluster compounds are seen to be uniformly distributed on the surface of the CNTs.
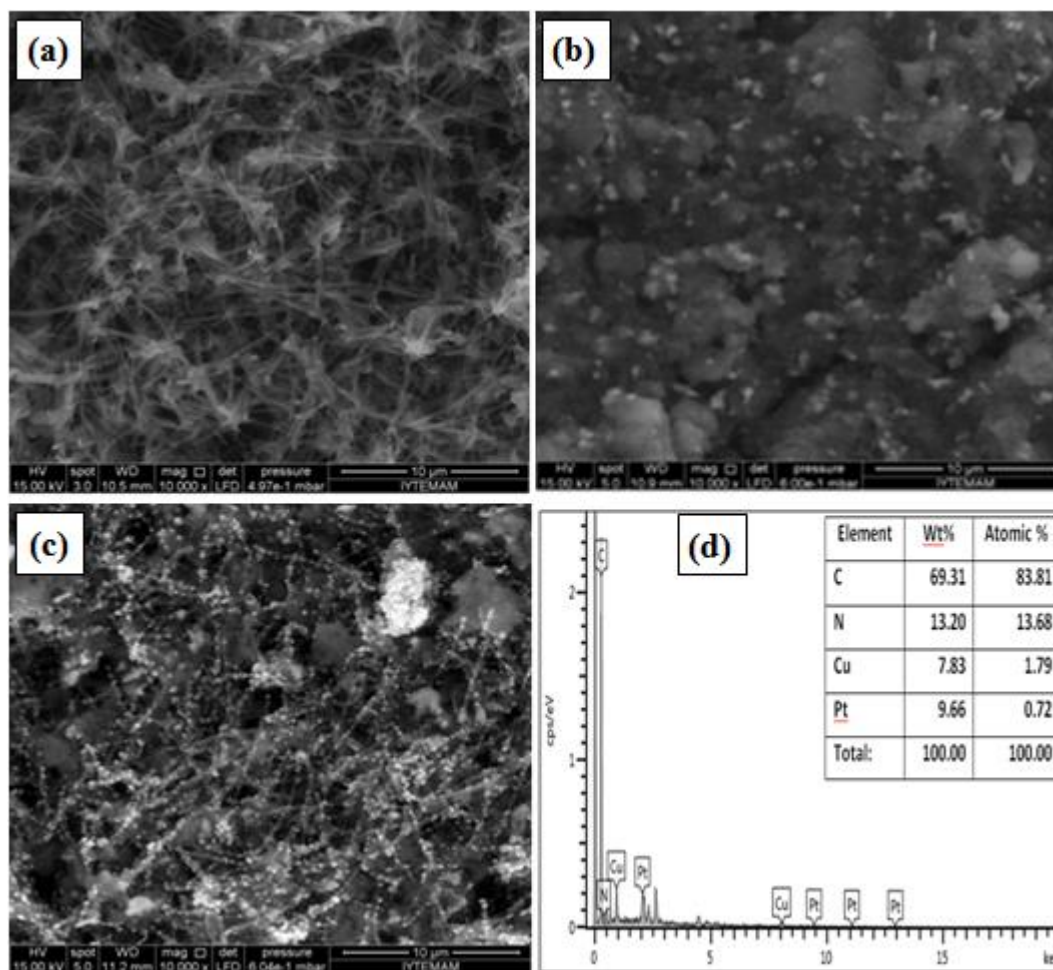
Figure 1. SEM images of a) CNT/GCE, b) CuPc-CNT/GCE, and c) PtNPs/CuPc-CNT/GCE; d) EDX spectra of PtNPs/CuPc-CNT/GCE.

The results imply that immobilization of copper Pc on the CNTs produced the uniform distribution of surface functional groups, which are beneficial to the deposition of PtNPs.[54−56]

On the other hand, comparison of SEM and TEM images indicated that the diameters of metal particles were not the same due to the dissimilar preparation of SEM and TEM sample procedures. In the SEM measurements the electrochemically prepared modified surface can be directly monitored with the SEM system without any additional operation and the original electrode surface is protected. On the other hand, in the case of TEM measurements, the content has to be scraped from the surface with a sharp knife after the preparation of modified electrodes and then transferred to ethanol solution. Thus, the metal particles could be released to the small particles compared to SEM conditions. Therefore, the metal particle sizes in SEM images were higher than in TEM images.

The formation of platinum nanoparticles on the copper Pc-CNT was also characterized using XPS, as shown in Figure 3. A compositional analysis of the electrochemically deposited films was conducted by XPS to identify the quality of the material. The signals of Cu2p at 933.79 eV, O1s at 533.12 eV, N 1s at 399.45 eV, C1s at 285.19 eV, and Pt 4f at 73.54 eV were also observed, due to the surface modification of CNTs and copper Pc (Figure 3a).
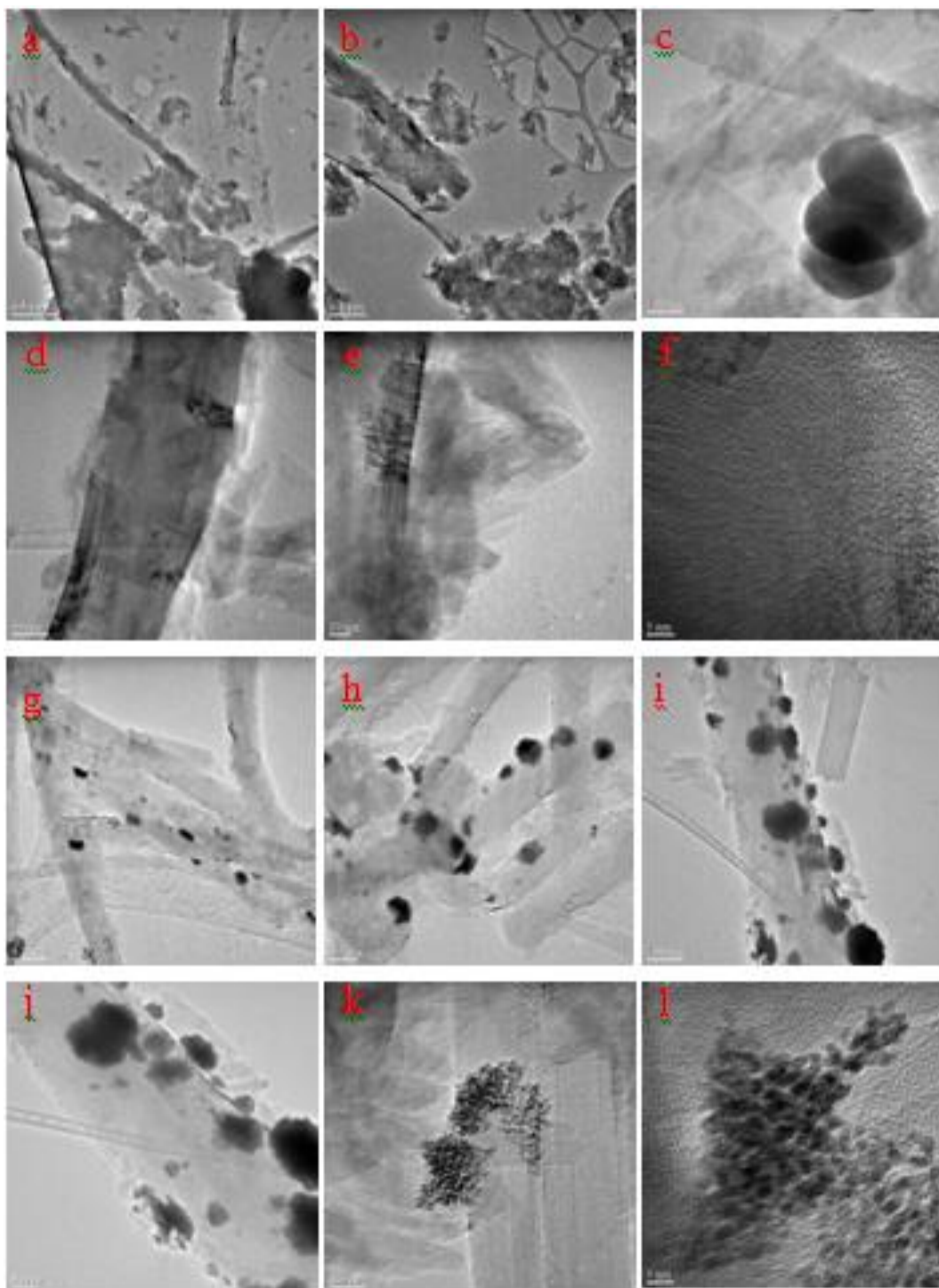
Figure 2. TEM images of samples at different magnifications: a–f) CuPc-CNT/GCE and g–l) PtNPs/CuPc-CNT/GCE.

Figure 3b shows the Pt 4f region of the XPS spectra of catalysts; the Pt 4f signal of the PtNPs/CNT/GCE catalysts can be fitted, and it shows that the two doublet peaks (due to spin-orbital splitting of the 4f7/2 and 4f5/2 states at 74.77 eV and 71.56 eV, respectively) can be attributed to metallic Pt. In addition, the $4f_{5/2}$
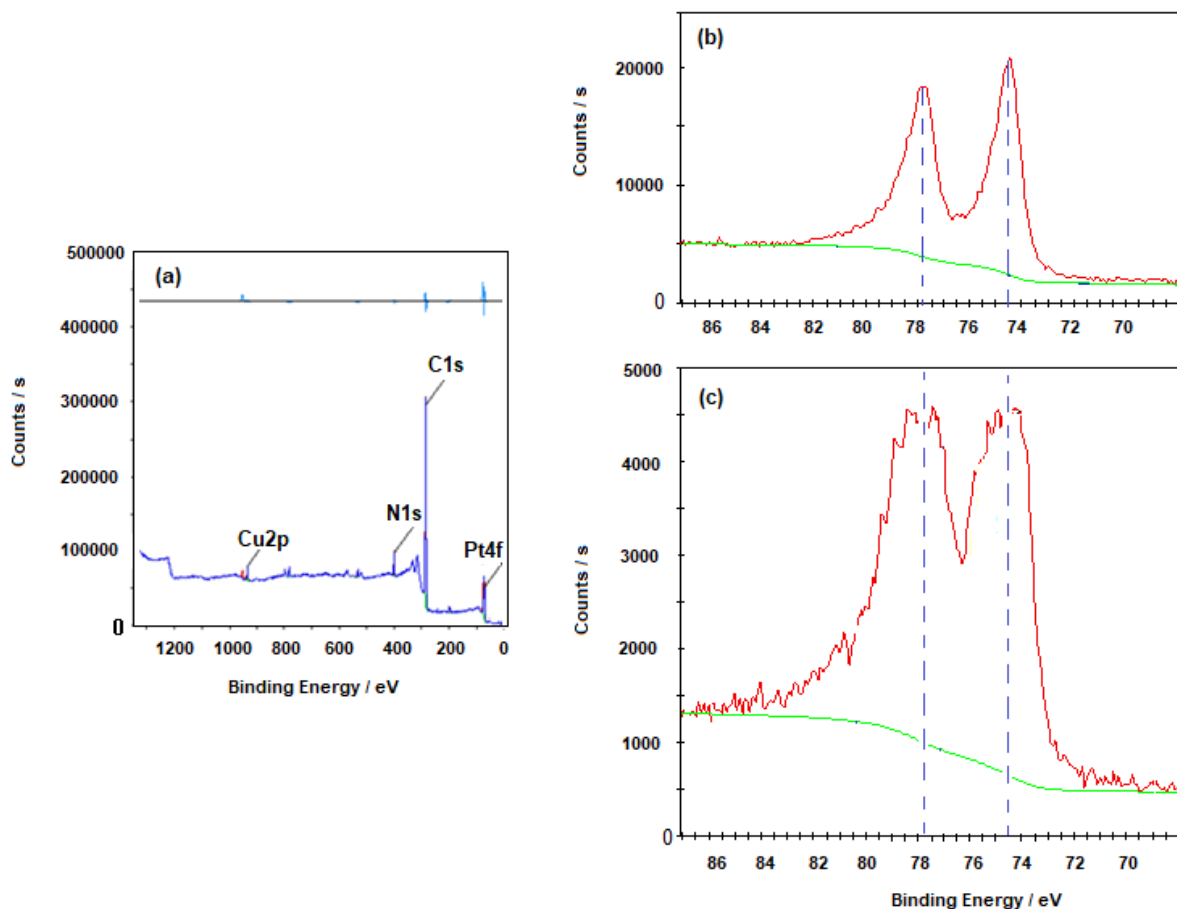
Figure 3. XPS spectra for a) survey of all elements, b) PtNPs/CNT/GCE, c) PtNPs/CuPc-CNT/GCE.

and $4f_{7/2}$ peaks have separation energies close to 3.21 eV.[57,58] In the literature, the peaks of Pt $4f_{7/2}$ at 72.8 eV and Pt $4f_{5/2}$ at 76.5 eV are attributed to the Pt^{2+} chemical state on PtO or $Pt(OH)_2$. However, the binding energy of Pt^0 on PtNPs/CuPc-CNT/GCE is observed at 75.42 eV and 72.31 eV, indicating a negative shift in the binding energy of Pt species on the PtNPs/CuPc-CNT/GCE surface (Figure 3c). The peaks have separation energies close to 3.11 eV, and this doublet can be attributed to metallic platinum.[43]

It is of note that the binding energy of Cu2p of CuPc-CNT/GCE was observed to be 955.61 eV and 935.86 eV, revealing that a negative shift in the binding energy of Cu2p species occurred after deposition of Pt nanoparticles on the CuPc-CNT/GCE surface (figure not shown). Therefore, the binding energy of Cu in the copper Pc molecule decreased in the presence of Pt; this may be attributed to the interaction between Pt and Cu. In addition, the peaks of O1s, N1s, and C1s also shifted to a positive direction in the presence of Pt.

X-ray diffraction (XRD) is widely used to analyze the configuration of molecules and their crystallographic structures. XRD patterns of CuPc-CNT and PtNPs/CuPc-CNT on indium tin oxide (ITO) glass were analyzed, and HighScore and the ACSD database program were used for phase identification of samples. Figure 4 shows the comparative XRD patterns of bare ITO, CuPc-CNT/ITO, and PtNPs/CuPc-CNT/ITO. Characteristic ITO peaks are determined to have broad form at about $22°$, a sharp peak at $30.6°$, and weak peaks at $2\theta = 35.5°$, $50.9°$, and $60.6°$, which correspond with reflections of (211), (222), (400), (440), and (622) cubic structured ITO

(Figure 4a). The results obtained are in agreement with the literature.[59] The XRD pattern in Figure 4b shows that the characteristic peaks for CuPc are determined at $2\theta = 6.78°$, $6.86°$, $9.18°$, $9.74°$, and $15.62°$; these peaks correspond to the (200) and (002) planes of the α-phase and the (101) plane of the β-phase, α-phase, and polymorphic phase, respectively.[60] The other major peaks are at $26.28°$ and $26.35°$, which indicated 50% and 13% intensities, respectively; the sharp diffraction peak at $26.35°$ indicates the characteristic hexagonal structure of carbon (ICSD, card no. 98-002-9123). In addition, weak peaks at around $43°$, $54°$, and $78°$ are identified as the C(100), C(004), and C(110) reflection of the hexagonal graphite structure. These data are in excellent agreement with results of previous studies.[61,62]
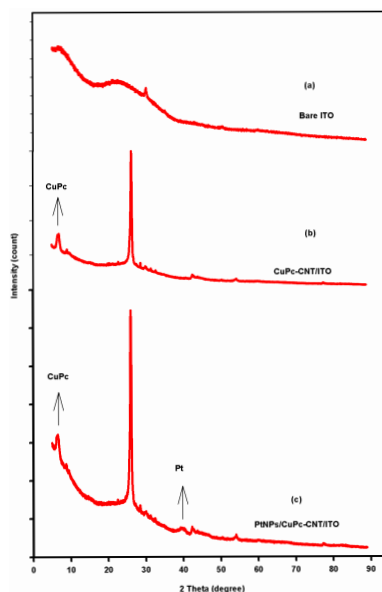

Figure 4. Comparative XRD patterns of bare and modified ITO electrodes.

XRD analysis confirmed that the Pt nanoparticles on the CuPc-CNT/ITO surface are pure metal nanoparticles, and the related pattern is shown in Figure 4c, where a sharp diffraction peak at $39.7°$ and weak broad diffraction peaks at $46.2°$ and $67.6°$ can be observed, corresponding to the (111), (200), and (220) crystalline planes of face-centered cubic Pt crystal, respectively. It is thus claimed that the Pt nanoparticles were formed of pure crystalline Pt. These results are also in good agreement with published available data.[63]

Figure 5 shows the results of EIS on bare GCE, CNT/GCE, CuPc/GCE, CuPc-CNT/GCE, and PtNPs/CuPc-CNT/GCE in the presence of 5 mM $K_3[Fe(CN)_6]/K_4[Fe(CN)_6]$/0.1 M KCl solution at varying frequencies from 0.05 to 50,000 Hz. The impedance circuit contains the solution resistance (Rs), Warburg impedance (W), constant phase element (CPE or Q), and charge transfer resistance (Rct). The Rct value is obtained from a semicircle diameter at high frequencies and relates to the dielectric and insulating characteristics of the electrode/electrolyte interface.[55] In Nyquist diagrams, a straight line with a slope of nearly $45°$ is related to the mass transport process via electroactive compound diffusion. Figure 5 clearly shows that the bare GCE has a large charge transfer resistance of about 548 Ω. The Rct value for the bare GCE is higher than the Rct values obtained for other modified electrodes; this low Rct value (1.7 Ω) for the PtNPs/CuPc-CNT/GCE implies a relatively fast charge transfer compared to the CNT/GCE (270 Ω), CuPc/GCE (62.3 Ω), CuPc-CNT/GCE (15.8 Ω), and bare GCE (548 Ω). The Rct value of bare GCE was in good agreement with the published data.[64]

These results suggest that the synergistic effect of CNTs with Pcs and Pt nanoparticles effectively increased the conductivity of the electrode and promoted the electron transfer rate.
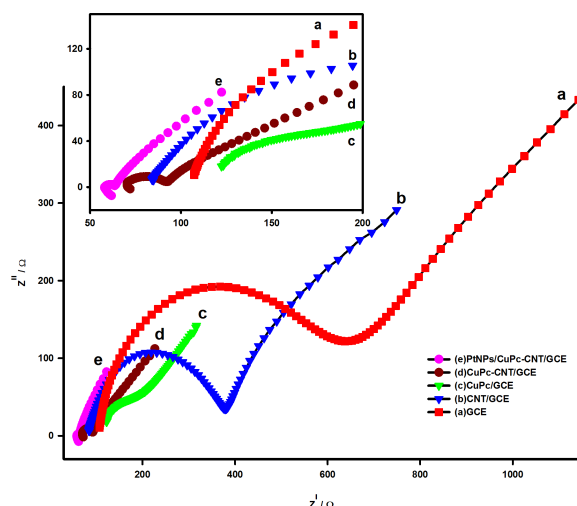

Figure 5. Nyquist plots for different electrodes of a) GCE, b) CNT/GCE, c) CuPc/GCE, d) CuPc-CNT/GCE, and e) PtNPs/CuPc-CNT/GCE in 5.0 mM $K_3[Fe(CN)_6]/K_4[Fe(CN)_6]$ (1:1) containing 0.1 M KCl solution at a frequency range of 0.05 to 50.000 Hz.

2.4. Oxygen reduction reaction on bare GCE and modified electrodes

The cyclic voltammograms of bare GCE and modified electrodes in 0.1 M NaOH solution with and without oxygen are shown in Figure 6. An oxygen reduction peak is observed at –436 mV with a 32 μA peak current on bare GCE but at –420 V with a 109 μA peak current on the CNT/GC electrode. This means the oxygen reduction peak current of CNT/GCE is more than 4.0 times higher than that of the bare GCE. However, it is observed at ca. –408 mV with a 32.5 μA peak current, –436 mV with a 36.4 μA peak current, and –375 mV with a 166 μA peak current for CuPc/CNT/GCE, CNT/CuPc/GCE, and CuPc-CNT/GCE, respectively. These results show that CuPc/CNT/GC and CNT/CuPc/GC electrodes prepared layer-by-layer have less catalytic activity during the ORR than CuPc-CNT/GCE, which was prepared using only a single step by mixing the CuPc and CNT at the same suspension. The best catalytic activity for oxygen reduction is obtained from CuPc-CNT/GCE and a significant current enhancement is observed for this, which is about 5.2 times higher than the bare GCE and 1.5 times higher than CNT/GCE.

To improve the electrocatalytic activity of composite electrodes in the reduction of oxygen, the electrodes were modified with platinum nanoparticles. Figure 7 shows the comparative CV results of oxygen reduction at Pt/GC, CuPc/GC, CNT/GC, and CuPc-CNT/GC electrodes modified with platinum nanoparticles and Pt disk. Oxygen reduction occurs at very negative potentials with a small peak on the Pt disk electrode (–207 mV with a 36.4 μA peak current) and at –180 mV with a 322 μA peak current on PtNPs/CNT/GCE. The PtNPs/CuPc-CNT/GCE shows a better response compared to the other electrodes, both in terms of peak current and peak potential. The peak current value at the PtNPs/CNT/GCE is 1.4, 5.8, and 8.7 times higher than for PtNPs/CNT/GCE, PtNPs/CuPc/GCE, and the Pt disk electrode, respectively. As expected, the PtNPs/CuPc-CNT/GC electrode showed a single peak, which could be attributed to the one-step four-electron reduction of

oxygen. This result agrees with the literature data as it is well known that the Cu–Au–MWCNT/GCE catalysts follow the direct four-electron pathway.[42]
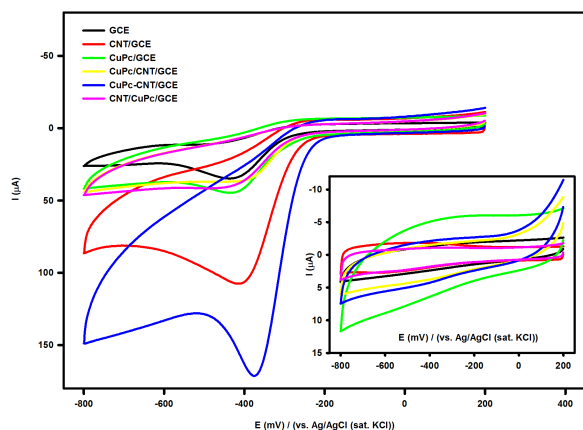

Figure 6. Cyclic voltammetric behavior of bare GCE, CNT, and CuPc different modified electrodes in O_2-saturated 0.1 M NaOH. Background voltammograms of electrodes are given in inset. Scan rate: 50 mV s^{-1}.
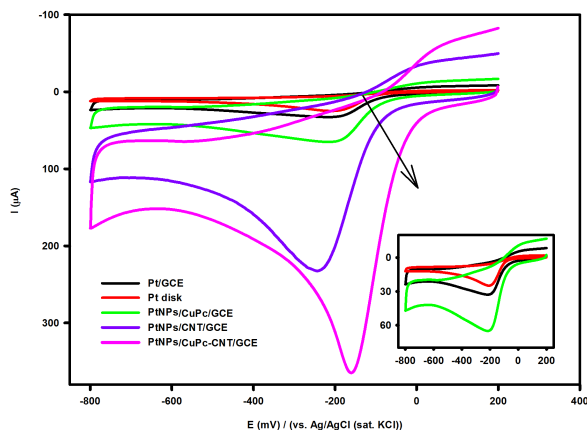
Figure 7. Cyclic voltammograms of oxygen reduction reaction on Pt disk, Pt/GCE, PtNPs/CuPc/GCE, Pt-NPs/CNT/GCE, and PtNPs/CuPc-CNT/GC electrodes in 0.1 M NaOH. Scan rate: 50 mV s^{-1}.

The effect of the concentration of NaOH on the electrocatalytic reduction of oxygen was also examined in a concentration range from 0.01 M to 1 M sodium hydroxide (not shown here). While the peak potential of oxygen slightly shifted to positive potentials, the peak current decreased with an increase in the NaOH concentration; this is considered to be related to the decrease in molecular oxygen solubility and diffusion coefficient and also to the gradual increase in sodium hydroxide viscosity. In addition, the slightly positive shift of the oxygen reduction peak potential could be attributed to the strong interaction between specific adsorption of OH^- anions and oxygen on the PtNPs/CuPc-CNT/GC electrode surface in an alkaline solution.[44] The overall results show that the best catalytic activity was observed at the PtNPs/CuPc-CNT/GC electrode in 0.1 M NaOH solution.

To observe the best catalytic effect of Pt nanoparticle-modified CuPc-CNT/GCE on oxygen reduction, the concentration of chloroplatinic acid solution was altered in a concentration range between 0.5 mM to 5 mM (figure not shown). With an increase in Pt^{4+} concentration, the oxygen reduction peak shifted to more positive potentials and the peak current increased. These results show that the best catalytic activity was observed at the PtNPs/CuPc-CNT/GC electrode prepared with 3 mM chloroplatinic acid solution. Therefore, future studies will be conducted using 3 mM chloroplatinic acid solution.

As it affects the characteristics of the oxygen reduction peak, it is necessary to optimize the CuPc:CNT mass ratio. Therefore, the amount of CuPc was altered to maintain a mass ratio of 1:15, 1:6, 1:2, and 1:1 CuPc:CNT, respectively, and the peak characteristics obtained from the resulting voltammograms are shown in Figure 8. The best response towards dissolved oxygen reduction was obtained with a mass ratio of 1:6 CuPc:CNT.

The effect of the scan rate on the peak current of oxygen reduction at all electrodes was studied in a range of 5–250 mV s^{-1}, where the peak current was increased linearly with the square root of the scan rate (figure not shown). This relationship was correlated with the characteristics of the diffusion-controlled process at the electrode surface.

2.5. Stability of PtNPs/CuPc-CNT film on electrode surface

The stability of the PtNPs/CuPc-CNT film modified electrode was studied by CV measurements; no remarkable change was observed in the current response of the modified electrode stored in the vapor of 0.1 M NaOH solution for 30 days. In addition, good reproducibility was observed for the modified electrode for ORR. The response of the electrode in a molecular oxygen saturated solution was maintained at 89.5% of the original peak current value after 30 days. A series of 10 modified electrodes was then prepared and used in the electrochemical reduction of oxygen for reproducibility of electrode. According to the results, relative standard deviation was found as only 3.5%. These experiments show that the GC electrodes modified with PtNPs/CuPc-CNT films have good reproducibility and stability, which is related to the good synergistic effect of the nanoparticles, CuPc, and CNT compounds.

2.6. Rotating-disk voltammetry

To determine the kinetic parameters more quantitatively, hydrodynamic voltammetric studies were also performed on rotating GC electrodes modified with PtNPs/CuPc-CNT, in both the absence and presence of oxygen in 0.1 M NaOH solution (Figure 9). RDE data were analyzed using the Koutecky–Levich (K–L) equation, which can be expressed as follows for a thin PtNPs/CuPc-CNT/GC on the electrode:[64−68]
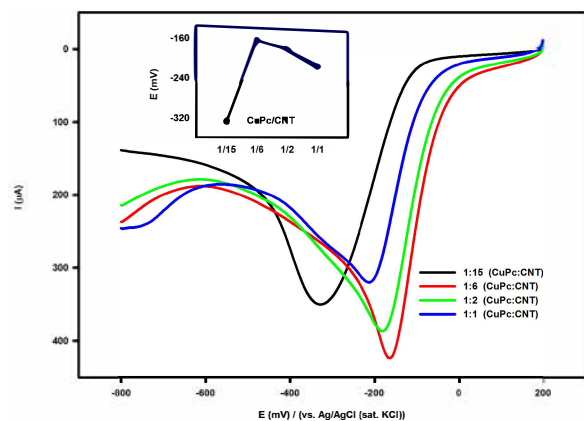

Figure 8. Linear sweep voltammograms of oxygen reduction at modified electrode with different CuPc:CNT mass ratios. Scan rate: 50 mV s^{-1}.
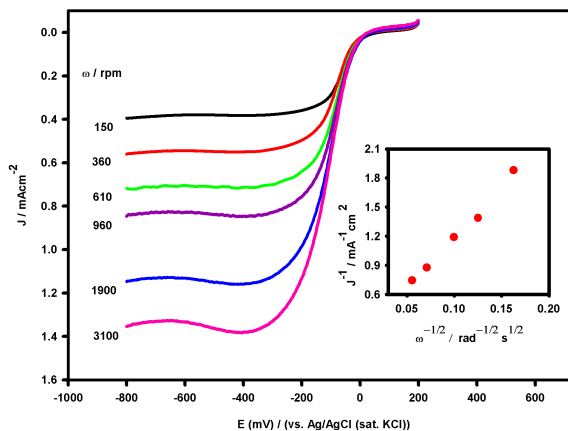
Figure 9. RDE voltammetry results for O_2 reduction on a PtNPs/CuPc-CNT/GC electrode in O_2-saturated 0.1 M NaOH. Inset: Koutecky–Levich plot for O_2 reduction.

$$\omega \frac{1}{j} = \frac{1}{j_k} + \frac{1}{B^{1/2}} \tag{4}$$

Here, j is the measured current density and j_k is the kinetic current density. The theoretical value of the Levich slope (B) is evaluated from Eq. (5) as follows:

$$B = 0.62 n F C_{O_2} D_{O_2}^{2/3} \gamma^{-1/6} \tag{5}$$

Here, n is the number of electrons transferred per oxygen molecule, F is the Faraday constant (96,500 C mol^{-1}), C_{O_2} is the concentration of oxygen in 0.1 M NaOH (1.2×10^{-6} mol cm^{-3}), D_{O_2} is the diffusion coefficient of

oxygen $(1.9 \times 10^{-5}$ cm^2 s$^{-1})$, and γ is the kinematic viscosity of the solution $(0.01$ cm^2 s$^{-1})$. According to Eq. (4), the plots of j^{-1} vs. $\omega^{-1/2}$ should be linear. From the slope of the K–L plots (inset in Figure 9), the value of n was calculated and determined to be 3.7 for the PtNPs/CuPc-CNT/GC electrode, indicating that O$_2$ was reduced by a direct almost four-electron pathway to produce water.

Many researchers studied the ORR by Pc-based electrodes besides other modifiers. A comparison between previously reported chemically modified electrodes for ORR is given in the Table. As can be seen, PtNPs/CuPc-CNT/GCE is a suitable catalyst for ORR as compared to the reduction potential. The electron number of the ORR was also compatible with the literatures, which was found as about 4, as desired (Table).

Table. Comparisons of the responses of oxygen reduction reaction constructed based on different modified electrodes.

Catalyst	Medium	Method	Ep (V)	n (electron number)	Ref.
FePc/C	0.1 M NaOH	CV	0.80 V (vs. RHE)	4.0	[46]
Pc-FePc/Mn-GCB	0.1 M KOH	CV	0.88 V (vs. RHE)	-	[47]
Fe$_2$Pc$_2$/GCE	0.1 M KOH	CV	–0.14 V (vs. SCE)	4.0	[48]
FePc/ERGO/ITO	0.1 M KOH	CV	–0.15 V (vs. SCE)	-	[49]
CoOx–FePc/C	50 mM PBS (pH 7)	CV	0.00 V (vs. SCE)	-	[50]
p-FePc/MWCNT	0.5 M H$_2$SO$_4$	CV	–0.13 V (vs. SCE)	-	[51]
Pt/MWCNT	0.1 M KOH	CV	0.80 V (vs. RHE)	4.0	[69]
Pt-Ru/C	0.1 M NaOH	CV	0.50 V (vs. Ag/AgCl)	4.0	[70]
PtSnP/C	50 mM PBS	CV	0.18 V (vs. Ag/AgCl)	-	[71]
Pt-Pd/CB	0.1 M PBS	CV	0.10 V (vs. Ag/AgCl)	-	[72]
Pt/CQDs	0.5 M H$_2$SO$_4$	CV	0.30 V (vs. Ag/AgCl)	3.8–4.1	[73]
Pt/Fe-N/R3DG	0.1 M KOH	CV	0.81 V (vs. RHE)	4.0	[74]
Pt/MoOx/GCE	0.1 M ABS (pH 5)	CV	0.25 V (vs. Ag/AgCl)	-	[26]
PtNPs/CuPc-CNT/GCE	0.1 M NaOH	CV	–0.18 V (vs. Ag/AgCl)	3.7	This work

FePc/C, Carbon-supported iron-phthalocyanine; Pc-FePc/Mn-GCB, iron(II) phthalocyanine on Mn-modified graphitized carbon black; Fe$_2$Pc$_2$, ball-type metallophthalocyanines with trifluoro methyl linkages; FePc/ERGO/ITO, iron phthalocyanine functionalized reduced graphene oxide on indium tin oxide; C–CoOx–FePc, carbon supported cobalt oxide modified iron phthalocyanine; p-FePc, poly-iron-phthalocyanine; Pt-Ru/C, carbon supported bimetallic Pt–Ru nanoparticles; PtSnP/C, PtSn with different Pt/Sn atomic ratios catalysts; Pt-Pd/CB, Pt–Pd deposited on carbon black; Pt/CQDs, Pt deposited on carbon quantum dots; Pt/Fe-N/R3DG, Pt nanoparticle modified Fe, N codoped robust 3D graphene; Pt/MoOx/GCE, Pt nanoparticles and molybdenum oxide modified glassy carbon electrode; CV, cyclic voltammetry; ABS, acetate buffer solution; PBS, phosphate buffer solution.

Mass-transport currents were used to examine the Tafel behavior of the mixed kinetic diffusion region (Figure 10). The Tafel slope varies from –0.056 V dec^{-1} (for lower current densities) to –0.11 V dec^{-1} (for the higher current densities) for bare and modified electrodes. Changing the coverage of the surface by adsorbed oxygen species gives rise to two Tafel slope regions, which are attributed to the change from Temkin to Langmuir conditions. This behavior was very similar to that observed with Cu-Au-MWCNT/GCE.[42]

2.7. Conclusions

The Pt nanoparticle-decorated CuPc-CNT composite electrode exhibited relatively higher electrocatalytic activity for ORR in terms of both reduction peak potential and peak current compared to the other prepared electrodes. The higher electrocatalytic activity may be attributed to the homogeneous dispersion and synergistic effect between Pt nanoparticles[26] and CuPc on the CNT/GCE surface. In addition, the ratio of CuPc:CNT was found to strongly affect the electrocatalytic activity of the electrode; according to these experiments, an
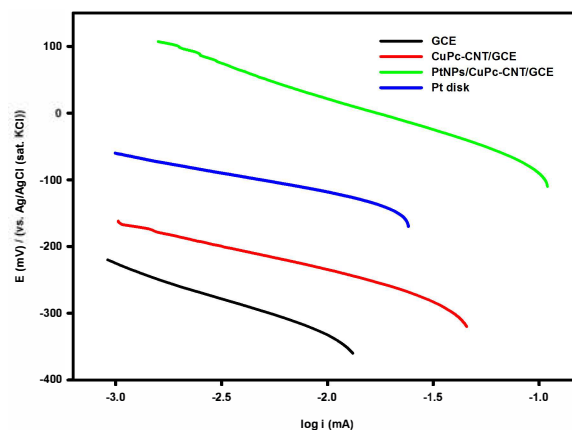
Figure 10. Tafel slopes of oxygen reduction on different electrode surfaces in 0.1 M NaOH for a 5 mV s^{-1} scan rate.

optimum ratio of 1:6 was determined. The surface characterization of the prepared electrodes was examined by SEM, TEM, XPS, XRD, and EIS. Furthermore, data analysis of the RDE showed that the reduction of oxygen on the PtNPs/CuPc-CNT/GC electrocatalysts followed a four-electron pathway. The results of this work show that PtNPs/CuPc-CNT/GCE is a suitable catalyst for ORR.

3. Experimental

A BAS 100B/W voltammetric analyzer (Bioanalytical Systems, Inc.) with a three-electrode system involving a working electrode (bare GCE with a diameter of 3 mm, 0.0707 cm^2 geometric area, CNT/GCE, CuPc/GCE, CuPc-CNT/GCE, and PtNPs/CuPc-CNT/GCE), a platinum wire counter electrode, and a Ag/AgCl (sat. KCl) reference electrode were used for voltammetric measurements. The surface characterization was examined using a ThermoK-Alpha-Monochromated High-Performance XPS spectrometer and FEI Quanta 250 FEG SEM, and TEM images were taken by a JEM-200F transmission electron microscope (JEOL).

XRD patterns of both bare and modified ITO were obtained by XRD analyses using a PANalytical Emperian diffractometer with Cu-K-α1 radiation (1.5406 Å; 45 kV, 40 mA); samples were scanned from 5 to 90 2θ in step sizes of 0.0130. XRD patterns were then matched using the PANalytical High Score program and ICSD database.

CNTs were purchased from Aldrich (multiwalled carbon nanotubes; purity >95%, diameter 110–170 nm, length 9 μm); chloroplatinic acid purchased from Sigma Aldrich was used to form Pt nanoparticles on the modified electrodes; N,N-dimethyl formamide (DMF), HNO$_3$, and HCl were all of ultrapure grade and purchased from Merck. Copper Pc (C$_{32}$H$_{16}$CuN$_8$) was purchased from Sigma-Aldrich (molecular weight: 576.07 g mol^{-1}, practically insoluble in water and alcohol and dispersed in DMF in this study); NaOH was obtained from Riedel-de Haën. All solutions were prepared using ultrapure water (Milli-Q 18.2 MΩ cm, Millipore).

3.1. Pretreatment of CNTs and preparation of modified electrodes

Before preparing the modified electrodes, the GCE was cleaned by polishing with a synthetic cloth and 0.05–3 μm Al$_2$O$_3$ slurry. The electrode was then ultrasonicated for 3 min in ethanol and pure water, respectively. Purification and activation procedures were applied to untreated CNTs using the following steps: 0.1 g of

CNT was boiled in an adequate amount of HNO_3, acid-treated CNTs were then rinsed with ultrapure water repeatedly,[42] and, finally, a black suspension was prepared by dispersing 30 mg of purified CNT in 4 mL of DMF. The CNT/GC electrode was prepared by dropping 10 μL of sample CNT suspension on the preconditioned GCE, and the solvent of the suspension on the GCE surface was then evaporated by placing and maintaining the electrode in an oven at 60 °C.

In addition, 4 mg of CuPc was dispersed in 4 mL of DMF to obtain a blue suspension. A sample of 10 μL of the CuPc suspension was then dropped onto the bare GC electrode surface and the solvent of the suspension was subsequently evaporated at 60 °C to fabricate the CuPc/GCE. The CuPc/CNT/GCE was prepared by dropping 5 μL of CuPc suspension after 5 μL of CNT suspension had been dropped on the bare GCE and dried at 60 °C, while the CNT/CuPc/GC electrode was prepared by reversing the procedure.

Furthermore, the CuPc-CNT suspension was also prepared by mixing 4 mg of CuPc with 30 mg of CNT in 4 mL of DMF; this dark blue suspension was then ultrasonicated for 60 min. A sample of 10 μL of CuPc-CNT mixture was dropped on the GCE surface and the modified electrode was subsequently dried at 60 °C to fabricate the CuPc-CNT/GCE. Before using the electrodes, all were rinsed thoroughly with ultrapure water. The experiments in an oxygen-free solution were performed under a high-purity N_2 gas atmosphere. Finally, the Pt metal nanoparticles were decorated on the composite electrode surface by an electrochemical reduction of K_2PtCl_6.

Acknowledgments

References

1. Chang, C. H.; Yuen, T. S.; Nagao, Y.; Yugami, H. *J. Power Sources* **2010**, *195*, 5938-5941.

2. Mao, J.; Yang, L.; Yu, P.; Wei, X.; Mao, L. *Electrochem. Commun.* **2012**, *19*, 29-31.

3. Wu, J.; Zhang, D.; Wang, Y.; Wan, Y. *Electrochim. Acta* **2012**, *75*, 305-310.

4. Zhang, F.; Saito, T.; Cheng, S.; Hickner, M. A.; Logan, B. E. *Environ. Sci. Technol.* **2010**, *44*, 1490-1495.

5. Yavuz, E.; Özdokur, K. V.; Çakar, İ.; Koçak, S.; Ertaş, F. N. *Electrochim. Acta* **2015**, *151*, 72-80.

6. Toccoli, T.; Boschetti, A.; Iannotta, S. *Synth. Met.* **2001**, *122*, 229-231.

7. Oni, J.; Nyokong, T. *Anal. Chim. Acta* **2001**, *434*, 9-21.

8. Lelievre, D.; Petit, M. A.; Simon, J. *Liq. Cryst.* **1989**, *4*, 707-710.

9. Claessens, C. G.; Hahn, U.; Torres, T. *Chem. Rec.* **2008**, *8*, 75-97.

10. Torre, G.; Claessens, C. G.; Torres, T. *Chem. Commun.* **2007**, *20*, 2000-2015.

11. Ishii, K. *Coord. Chem. Rev.* **2012**, *256*, 1556-1568.

12. Lo, P. C.; Leng, X.; Ng, D. K. P. *Coord. Chem. Rev.* **2007**, *251*, 2334-2353.

13. Meenakshi, S.; Pandian, K.; Jayakumari, L. S.; Inbasekaran S. *Mater. Sci. Eng. C* **2016**, *59*, 136-144.

14. Sharma, A. K.; Mahajan, A.; Saini, R.; Bedi, R. K.; Kumar, S.; Debnathd, A K.; Aswal, D. K. *Sens. Actuat. B* **2018**, *255*, 87-99.

15. Jeevagan, A. J.; John, S. A. *Electrochim. Acta* **2012**, *77*, 137-142.

16. Chen, A.; Kong, A.; Fan, X.; Yang, X.; Li, C.; Chen, Z.; Shan Y. *Int. J. Hydrogen Energ.* **2017**, *42*, 16557-16567.

17. Dursun, Z.; Gelmez, B. *Electroanalysis* **2010**, *22*, 1106-1114.

18. Dasgupta, K.; Joshi, J. B.; Banerjee, S. *Chem. Eng. J.* **2011**, *171*, 841-869.

19. Ma, P. C.; Siddiqui, N. A.; Marom, G.; Kim, J. K. *Compos. Part A-Appl. S.* **2010**, *41*, 1345-1367.

20. Koçak, S.; Aslışen, B. *Sens. Actuat. B* **2014**, *196*, 610-618.

21. Wildgoose, G. G.; Banks, C. E.; Leventis, H. C.; Compton, R. G. *Microchim. Acta* **2006**, *152*, 187-214.

22. Mugadza, T.; Nyokong, T. *Polyhedron* **2011**, *30*, 1820-1829.

23. Costamagna, J.; Ferraudi, G.; Matsuhiro, B.; Campos-Vallette, M.; Canales, J.; Villagran, M. *Coord. Chem. Rev.* **2000**, *196*, 125-164.

24. Torre, G.; Blau, W.; Torres, T. *Nanotechnology* **2003**, *14*, 765-771.

25. Moraes, F. C.; Golinelli, D. L. C.; Mascaro, L. H.; Machado, S. A. S. *Sens. Actuat. B* **2010**, *148*, 492-497.

26. Çakar, İ.; Özdokur, V. K.; Demir, B.; Yavuz, E.; Demirkol, D. O.; Koçak, S.; Timur, S.; Ertaş, F. N. *Sens. Actuat. B.* **2013**, *185*, 331-336.

27. Karabiberoğlu, Ş. U.; Dursun, Z. *J. Solid State Electrochem.* **2016**, *20*, 2009-2018.

28. Katz, E.; Willner, I.; Wang, J. *Electroanalysis* **2004**, *16*, 19-44.

29. Hernandez-Santos, D.; Gonzalez-Garcia, M. B.; Garcia, A. C. *Electroanalysis* **2002**, *14*, 1225-1235.

30. Welch, C. M.; Compton, R. G. *Anal. Bioanal. Chem.* **2006**, *384*, 601-619.

31. Raj, C. R.; Okajima, T.; Ohsaka, T. *J. Electroanal. Chem.* **2003**, *543*, 127-133.

32. Lu, Y.; Reddy, R. G. *Int. J. Hydrogen Energy* **2008**, *33*, 3930-3937.

33. Tsai, M. C.; Yeh, T. K.; Tsai, C. H. *Int. J. Hydrogen. Energy* **2011**, *36*, 8261-8266.

34. Du, H. Y.; Wang, C. H.; Hsu, H. C.; Chang, S. T.; Chen, U. S.; Yen, S. C. *Diamond Relat. Mater.* **2008**, *17*, 535-541.

35. Siracusano, S.; Stassi, A.; Baglio, V.; Arico, A. S.; Capitanio, F.; Tavares, A. C. *Electrochim. Acta* **2009**, *54*, 4844-4850.

36. Xiong, L.; Manthiram, A. *Electrochim. Acta* **2005**, *50*, 2323-2329.

37. Chang, C. H.; Yuen, T. S.; Nagao,Y.; Yugami, H. *Solid State Ionics* **2011**, *197*, 49-51.

38. Wang, Z.; Zhang, Q.; Kuehner, D.; Xu, X.; Ivaska, A.; Niu, L. *Carbon* **2008**, *46*, 1687-1692.

39. Lin, A. S.; Huang, J. C. *J. Electroanal. Chem.* **2003**, *541*, 147-151.

40. Sljukic, B.; Banks, C. E.; Compton, R. G. *J. Iranian Chem. Soc.* **2005**, *2*, 1-25.

41. Ko, A. R.; Lee, Y. W.; Moon, J. S.; Han, S. B.; Cao, G.; Park, K. W. *Appl. Catal. A* **2014**, *477*, 102-108.

42. Bakir, Ç. C.; Şahin, N.; Polat, R.; Dursun, Z. *J. Electroanal. Chem.* **2011**, *662*, 275-280.

43. Dursun, Z.; Karabiberoğlu, Ş. U.; Gelmez, B.; Ertaş, F. N. *Turk. J. Chem.* **2011**, *35*, 513-521.

44. Dursun, Z.; Ulubay, Ş.; Gelmez, B.; Ertaş, F. N. *Catal. Lett.* **2009**, *132*, 127-132.

45. Prasad, K. S.; Chuang, M. C.; Ho, J. A. *Talanta* **2012**, *88*, 445-449.

46. Hebié, S.; Bayo-Bangoura, M.; Bayo, K.; Servat, K.; Morais, C.; Napporn, T. W.; Kokoh, K. B. *J. Solid State Electrochem.* **2016**, *20*, 931-942.

47. Zhang, Z.; Dou, M.; Ji, J.; Wang, F. *Nano Energy* **2017**, *34*, 338-343.

48. Koçyigit, N.; Özen, Ü. E.; Özer, M.; Salih, B.; Özkaya, A. R.; Bekaroglu, Ö. *Electrochim. Acta* **2017**, *233*, 237-248.

49. Liu, D.; Long, Y. T. *ACS Appl. Mater. Interface* **2015**, *7*, 24063-24068.

50. Ahmed, J.; Yuan, Y.; Zhou, L.; Kim, S. *J. Power Sources* **2012**, *208*, 170-175.

51. Peng, Y.; Li, Z.; Xia, D.; Zheng, L.; Liao, Y.; Li, K.; Zuo, X. *J. Power Sources* **2015**, *291*, 20-28.

52. Konopka, S. J.; McDuffie, B. *Anal. Chem.* **1970**, *42*, 1741-1746.

53. Carvalho, R. C.; Gouveia-Caridade, C.; Brett, C. M. A. *Anal. Bioanal. Chem.* **2010**, *398*, 1675-1685.

54. Qing, X.; Shi, J.; Ma, C.; Fan, M.; Bai, Z.; Chen, Z. *J. Power Sources* **2014**, *266*, 88-98.

55. Chen, Y.; Zhang, G.; Ma, J.; Zhou, Y.; Tang, Y.; Lu. T. *Int. J. Hydrogen Energy* **2010**, *35*, 10109-10117.

56. Jin, X.; He, B.; Miao, J.; Yuan, J.; Zhang, Q.; Niu, L. *Carbon* **2012**, *50*, 3083-3091.

57. Acharya, C. K.; Li, W.; Liu, Z.; Kwon, G.; Turner, C. H.; Lane, A. M. *J. Power Sources* **2009**, *192*, 324-329.

58. Ji, Z. G.; Wong, K. W.; Wang, M.; Tse, K. P. K.; Kwok, R. W. M.; Lau, W. M. *Nucl. Instrum. Meth. B* **2001**, *174*, 311-316.

59. Koo, J.; Jung, J. Y.; Lee, S.; Lee, M.; Chang, J. *Marine Pollut. Bull.* **2015**, *98*, 130-136.

60. Afify, H. A.; Gadallah, A. S.; El-Nahass, M. M.; Khedr, M. A. *J. Molec. Struct.* **2015**, *1098*, 161-166.

61. Atchudan, R.; Perumal, S.; Immanuel, E. T. N. J.; Pandurangan, A.; Lee, Y. R. *Physica E* **2015**, *74*, 355-362.

62. Zeng, J. Q.; Sun, S. N.; Zhong, J. P.; Li, X. F.; Wang, R. X.; Wu, L. N.; Wang, L.; Fan, Y. J. *Int. J. Hydrogen Energy* **2014**, *39*, 15928-15936.

63. Sharma, R.; Kar, K. K. *Electrochim. Acta* **2015**, *156*, 199-206.

64. Gholivand, M. B., Solgi, M. *Electrochim. Acta* **2017**, *246*, 689-698.

65. Erikson, H.; Kasikov, A.; Johans, C.; Kontturi, K.; Tammeveski, K.; Sarapuu, A. *J. Electroanal. Chem.* **2011**, *652*, 1-7.

66. Mamuru, S. A.; Ozoemena, K. I.; Fukuda, T.; Kobayashi, N.; Nyokong, T. *Electrochim. Acta* **2010**, *55*, 6367-6375.

67. Prakash, J.; Joachin, H. *Electrochim. Acta* **2000**, *45*, 2289-2296.

68. Morozan, A.; Campidelli, S.; Filoramo, A.; Jousselme, B.; Palacin, S. *Carbon* **2011**, *49*, 4839-4847.

69. Hussain, S.; Erikson, H.; Kongi, N.; Merisalu, M.; Ritslaid, P.; Sammelselg, V.; Kaido, T. *Int. J. Hydrogen Energy* **2017**, *42*, 5958-5970.

70. Hosseini, M. G.; Zardari, P. *Appl. Surf. Sci.* **2015**, 345, 223-231.

71. Li, B.; He, Z.; Wang, M.; Wang, X. *Int. J. Hydrogen Energy* **2017**, *42*, 5261-5271.

72. Lee, Y. W.; Oh, S. E.; Park, K. W. *Electrochem. Commun.* **2011**, *13*, 1300-1303.

73. Kakaei, K. *Int. J. Hydrogen Energy* **2017**, *42*, 11605-11613.

74. Qin, Y.; Chao, L.; He, J. J.; Liu, Y.; Chu, F.; Cao, J.; Kong, Y.; Tao, Y. *J. Power Sources* **2016**, *335*, 31-37.